Electrochimica Acta 218 (2016) 335–344

Contents lists available at ScienceDirect

Electrochimica Acta

journal homepage: www.elsevier.com/locate/electacta

Nanofiber Carbon-Supported Phthalocyanine Metal Complexes as Solid Electrocatalysts for Lithium-Air Batteries

Anupriya Arul[a], Maria Christy[b], Mi Young Oh[b], Yun Sung Lee[c,*], Kee Suk Nahm[a,b,*]

[a] Department of Energy Storage & Conversion Engineering, Chonbuk National University, Jeonju 561-756, Republic of Korea
[b] R&D Education Centre for Fuel Cell Materials & Systems, and School of Chemical Engineering, Chonbuk National University, Jeonju 561-756, Republic of Korea
[c] Faculty of Applied Chemical Engineering, Chonnam National University, Gwangju 500-757, Republic of Korea

ARTICLE INFO

Article history:
Received 14 January 2016
Received in revised form 24 September 2016
Accepted 25 September 2016
Available online 27 September 2016

Keywords:
Electrocatalysts
phthalocyanines
graphite nanofibers
oxygen reduction
oxygen evolution

ABSTRACT

Iron phthalocyanine supported on graphite nanofibers (GNF_FePc) were synthesized using a simple solvothermal process and characterized using various structural analyses. GNF_FePc were employed as bifunctional electrocatalysts in the air cathode of lithium-oxygen batteries. Galvanostatic charge–discharge tests, cyclic voltammetry, and electrochemical impedance spectroscopy were performed to assess the Performance of Li-air batteries. The air-cell delivered a high specific capacity of ~5500 mAh/g at the first cycle which remained close to 90% of that value after 4 cycles. The reversibility was nearly 100% for all the four cycles with comparatively lower over potential.

1. Introduction

A lithium–Oxygen (Li–O_2) battery possesses qualities that could positively replace gasoline with its very high specific energy. Yet, for practical applications, there are hurdles to overcome which include reduced cell capacity resulting in low reversibility and cyclability, and high overpotential [1–4]. Basically, all of these problems occur during the charge–discharge process of the cell, mainly due to reactions at interfaces on oxygen electrocatalysts in the air cathode [5,6]. So the selectivity of an air-cathode catalyst plays a crucial role in the performance of the battery [7]. However, an air cathode also determines the power and energy density of the battery depending on the material being used. Hence it is of utmost importance to develop proper and stable electrocatalysts for the air cathode of Li–O_2 batteries. A typical air cathode catalyst should be bifunctional in order to catalyze both oxygen reduction reaction (ORR, the forward reaction) and the oxygen evolution reaction (OER, the reverse reaction), which results in the formation and decomposition of the reaction product Li_2O_2. In other words, the electrocatalyst must promote the proper formation and decomposition of the reaction product (Li_2O_2) and suppress the formation of any other reaction products that could not be sustainably recharged.

Numerous electrocatalysts have been investigated as the air cathode in prior studies eg, noble metal catalysts (Pt, Au, Pd), non–precious metals (Co, Fe, Cu), transition metal oxides (TiO_2, RuO_2, MnO_2) and carbon-based catalysts, etc., [8–12]. The long-term performance target for a Li-air battery requires a carbon loading of 1.0 mg cm^{-2} that corresponds to a power density of ~25 mW cm^{-2} [13,14]. The low-rate capability (in mA cm^{-2}) of a Li-air battery is the main reason for its high-catalyst usage. Within that context, the possibility of using noble-metal catalysts for long-term or practical applications seems impossible [13]. Other catalysts utilizing non–precious metals and transition metal oxides have been reported to have improved discharge voltages and rate capabilities [15–20]. However, the termination of the cell process after a few cycles occurs due to various reasons. Similar problems have also been reported with carbon-based catalyst, although carbon has been widely used for this purpose. Nevertheless, carbon is an excellent electrocatalytic support with high porosity and electronic conductivity [21–24]. Ongoing investigations are focused on overcoming the above mentioned practical concerns in various electrocatalysts. A proper understanding of materials

* Corresponding author.
E-mail addresses: leeys@chonnam.ac.kr (Y.S. Lee), nahmks@jbnu.ac.kr (K.S. Nahm).

http://dx.doi.org/10.1016/j.electacta.2016.09.131
0013-4686/

and their physical chemistry are mandatory to develop a stable oxygen electrocatalyst with improved energy efficiency.

Phthalocyanines (Pc) are purely synthetic ligands, structurally related to porphyrin complexes but comparatively cheap and readily accessible in large quantities. Metal Pc complexes are widely studied for their catalytic aerobic oxidations, reduction and destruction of peroxides. Metal Pc are considered to be suitable oxygen catalysts based on their structural characteristics and accessibilities [25,26]. Metal Pchave received much attention due to the electrocatalytic reduction of O_2 while electrocatalytic reduction of O_2 is important in air cells. Several literature reports have commented on the catalytic properties of metal Pc [27–33]. Although it has been closely studied as catalysts, their catalytic chemistries in terms of mechanisms involved in these catalytic oxidations have yet to be detailed. By appropriate structural modifications of the metal Pc, the catalytic properties could be fine-tuned. Since the catalytic properties depend on the central metal in a complex structure. Iron phthalocyanine (FePc) has been mentioned as a catalyst layer and an oxygen sensor in air batteries [34]. FePc is an oxygen carrier which could enhance the solubility of oxygen and facilitate a reaction mechanism in the Li-O_2 battery. FePc, with its high electrocatalytic activity for ORR, performs better than other Metal Pc. [28,33].

In this work, FePc was combined with graphite nanofibers (GNF) to form mesoporous cathode catalysts by a simple solvothermal method, and the catalytic activities of GNF_FePc were systematically analyzed in a Li–air battery. The synthesized electrocatalysts showed good surface properties and electrocatalytic activities. The GNF_FePc catalyzed cathode exhibited better performance with significantly improved cyclability and low overpotential compared to the cathode without any catalyst. The manuscript analyzes all the physical and electrochemical properties of synthesized electrocatalysts. The ball-milling effect of FePc has been investigated as well.

2. Experimental

2.1. Sample preparation

Iron phthalocyanines (FePc, 90% purity) were purchased from Sigma-Aldrich (USA) and used without further purification. Graphite nanofibers (GNF) materials were commercially purchased (Carbon nanomaterial technology, co., Ltd. South Korea) and treated with 96.8 ml sulfuric acid and 42 ml nitric acid before being utilized for any further processes. GNF_FePc composites were prepared by a simple 3 step process via $\pi-\pi$ interactions. The $\pi-\pi$ interaction is the molecule-carbon interaction that occurs between the aromatic structure of the carbon surface and the macrocyclic ligand of the complex. The first step was to prepare FePc and GNF solutions by adding two equivalent amounts (40 mg) of FePc and GNF, respectively, in 100 ml dimethylformamide (DMF) solvent. The FePc solution was then added dropwise into the GNF dispersion under continuous stirring. The suspension was stirred for 7 hours at room temperature and then ultrasonicated for 40 mins. Finally, the GNF_FePc composite was washed with DMF and vacuum-dried at 80 °C. To see the effect of ball milling, FePc was ball–milled (BM), and the GNF_BM FePc composite was synthesized with the BM FePc using the above-mentioned 3-step process. For ball–milling, 1 g of FePc was taken with the sample to ball ratio of 1:50 in a ball-miller reactor and the mixture was ball-milled at 250 rpm for 1 hour.

2.2. Structural analysis

The phase identification of the synthesized samples was determined by powder x–ray diffraction, (XRD, Shimadzu XRD-6000, Japan) using a CuKα (λ = 1.54059 Å) target in the 2θ range of 10∼80°. The morphology of synthesized samples was examined with field emission scanning electron microscopy (FESEM, JSM–6700F, Japan) and the chemical composition of the sample was investigated with energy dispersive X–ray spectroscopy (EDAX) equipped in FESEM. The Brunauer–Emmett–Teller (BET) surface-area analysis of the materials was obtained using a nitrogen adsorption instrument (BEL SORP Bell Japan Inc., Japan). All the samples were degassed for 3 h at 300 °C under vacuum before performing surface-area measurements. Raman spectroscopy (3D Laser Raman Microspectroscopy System Nanofinder®–30 (Tokyo Instruments, Inc, Japan) was also performed to identify the molecules by their vibrational frequencies in the range of 5–3000 cm^{-1}. Fourier transform infrared spectroscopy (FTIR) was performed using a Perkin-Elmer instrument, Spectrum GX FT–IR system operating in the region of 400–4000 cm^{-1}. Thermal stability was examined via thermogravimetric analysis (TGA) (Thermo plus EV02, Rigaku Instruments, Japan), which was performed in N_2 atmosphere at a flow rate of 5 °C min^{-1} with a heating rate of 800 °C.

2.3. Electrochemical analysis

For electrochemical characterization studies, the air cathodes are prepared by mixing the synthesized catalyst and Ketjenblack (KB; EC 600JD) conductive carbon in the ratio of 1:2 with a teflonised acetylene black (TAB) binder (60%) in isopropyl alcohol. The mixture is prepared into a fine pellet of about 1 cm diameter, and the pellet is pressed on a Ni-mesh current collector with a diameter of 1.2 cm. The as-prepared electrode is used as an air cathode in a Li-O_2 cell after vacuum dried at 100 °C, overnight. A home-made Swagelok™ type Li-O_2 cell is composed of Li metal anode and the prepared air cathode in non-aqueous 1 M LiTFSI (99% TEGDME) electrolyte. Each cell is assembled in an argon-filled glove box under room temperature and purged with oxygen before testing the battery performance. The Swagelok™ type lithium-air battery is used in a non-aqueous medium for battery testing, electrochemical impedance spectrometry (EIS) and cyclic voltammetry (CV) measurements.

The galvanostatic testing of the Li–O_2 cell was performed in a computer-controlled BTS 2000 system (Japan) in the potential range of 2 – 4.3 V under O_2 flow at 1 atmosphere (atm). The interfacial impedances of air-cathodes were determined from EIS measured at a frequency range of 0.1 – 10^5 Hz by a computer-controlled Solatron analytical cell test system (Model 1470E, UK). Cyclic voltammetry was recorded in the range of 1.5 – 4.7 V vs. Li at a scan rate of 0.01 mV s^{-1} using a MultiStat computer controlled program.

3. Results and Discussion

3.1. Physical properties

Fig. 1(a) shows the X-ray diffraction (XRD) patterns of FePc, BM FePc, GNF and the synthesized catalysts ie, GNF_FePc and GNF_BM FePc. From the XRD spectrum of FePc (the very bottom spectrum), the sharp peaks are observed at 7.0, 9.2, 18.2, 18.6, 23.9, 26, 28, 29.6, 30.6°, which are well-indexed to characteristic planes (110), (102), (302), (104), (105), (401), (314), (215), (315) of FePc, respectively, [JCPDS No.14-0926] [35]. However, after ball milling, the FePc diffraction peaks are much lower in intensity to form few broad peaks at 7.2° and 22−27° respectively, as reported in the literature [36]. The broadening of the XRD peaks reveals, the loss of FePc crystallinity due to severe plastic deformation induced by high energy ball milling impacts [37]. No new peak was found in the pattern and no new structure was formed during milling. GNF

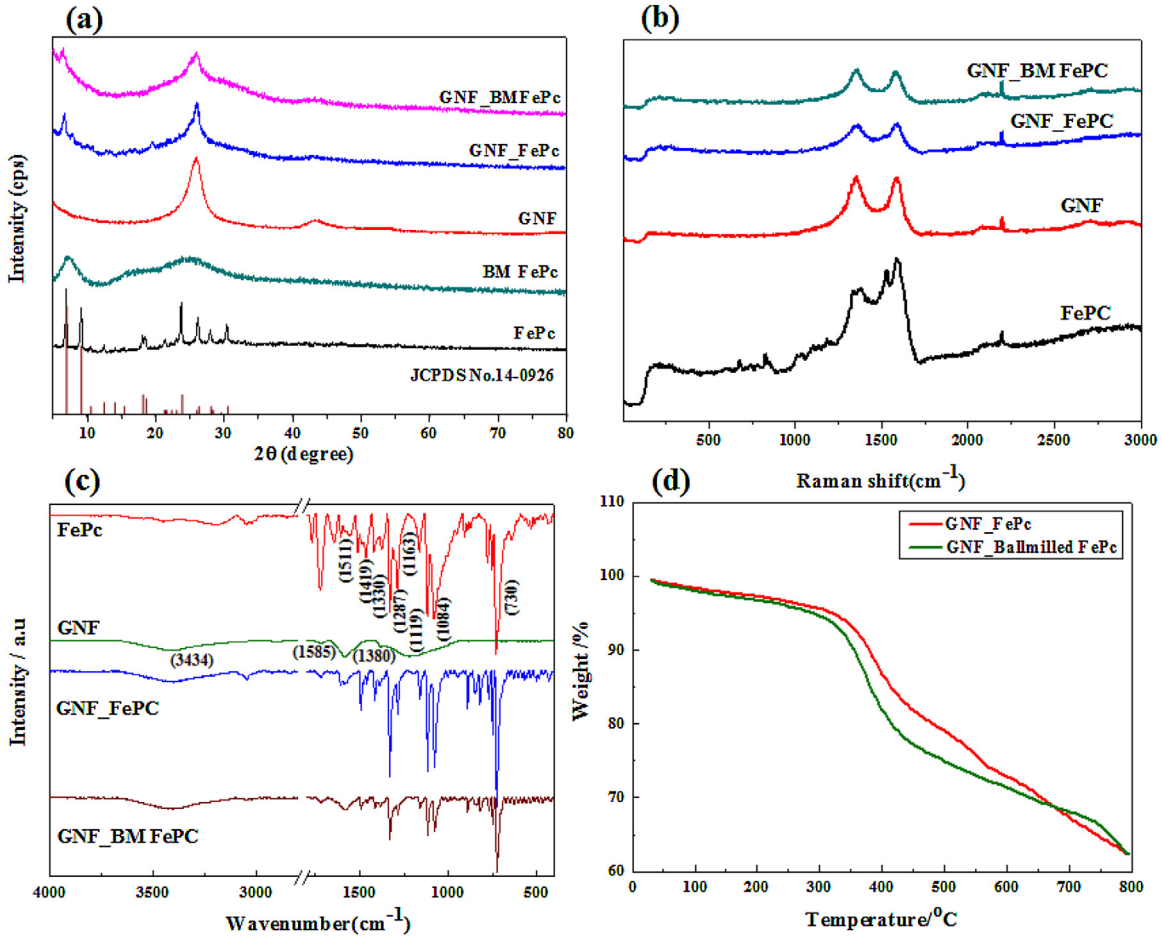

Fig. 1. (a) X–ray diffraction pattern, (b) Raman spectra, (c) Fourier transform infrared spectra and (d) thermogravimetric analysis of FePc, GNF, and the prepared GNF_FePc composites.

exhibited diffraction peaks at 2θ = 26 and 43°, which correspond to graphitic planes of (002) and (100) [38]. Synthesized composites such as GNF_FePc and GNF_BM FePc possess both the characteristic peaks of phthalocyanine and carbon. The inclusion of these characteristic peaks in the XRD patterns is evidence for the successful synthesis of iron phthalocyanine on GNF without any other impurities. Moreover, the FePc peak at 7° appears due to a molecular aggregate of FePc. The broadening of the peak observed in the synthesized composites shows that FePc molecule on carbon is less aggregated [36].

Raman spectroscopy and Fourier transform infrared spectroscopy are two other techniques that could be used to provide a characteristic fingerprint for the purpose of identifying synthesized materials. Raman spectra of the synthesized composite materials and references viz. FePc, GNF, GNF_FePc and GNF_BM FePc are shown in Fig. 1 (b). From Fig. 1 (b) characteristic D and G bands around 1336 and 1583 cm^{-1}, respectively for GNF and FePc could be clearly seen. The D band could be associated with structural defects and G band to the E_{2g} vibration mode of Sp^2 carbon domains. The intensity of the D band was found to vary from 1336 cm^{-1} to 1378 cm^{-1} and the G band was found to be ~1583 cm^{-1} [39]. The decrease in intensity for GNF_FePc and GNF_BM FePc demonstrated a successful formation of GNF_FePc composites. Strong bonding and crystallinity of substances were clear, and the I_D/I_G ratio of GNF and GNF_FePc was almost similar. This result indicated that the interaction between FePc and GNF did not destroy the conjugations of GNF.

The infrared spectra of synthesized phthalocyanines are given in Fig. 1(c). The presence of C—O at 1065, C—O—C at 1225, C=C at 1620 and C=O at 1740 cm^{-1} represented the GNF. Three strong peaks in the region 1000–1200 cm^{-1}, showing characteristic metal phthalocyanines could be seen from Fig. 1 (c). The spectral patterns in this region strongly depend on the molecular structure of the complexes and its chemical structure for the central metal, in this case, Fe. The middle peak originated from the vibration mode of a pyrrole ring, and the other two peaks are assigned to the in–plane deformation vibration of C—H bending in the ring [39]. The bands at 1506, 1415, 1329, 1285, 1161, 1117, 1079 and 719 cm^{-1} also indicated the presence of FePc. The band appearing at 1609 ± 3 cm^{-1} was assigned to the C—C stretching vibration in pyrrole and those bands appearing at 1428 ± 6 and 1332 ± 6 cm^{-1} were assigned to C—C stretching in isoindole. Also, the band appearing at 625 ± 9 cm^{-1} was assigned to a C—C macrocycle ring deformation. The bands appearing at 1284 ± 6, 1162 ± 4 and 1070 ± 11 cm^{-1} were assigned to the C—N in isoindole in-plane band in pyrrole stretching vibration, respectively.

TGA analysis of the materials was studied in N_2 atmosphere with a heating rate of 5 degrees/min up to 800 °C as shown in Fig. 1 (d). TGA was mainly used to find the thermal stability and to calculate the amount of iron phthalocyanine present on graphite nanofiber. From the mass percentage of TGA curves at 800 °C, it is evident that almost 63% of FePc was present in both GNF_FePc and GNF_BM FePc electrocatalysts. Regarding the stability of the materials, GNF_FePc appeared to be more stable than a ball-milled

catalyst since the former showed its first thermal decomposition at 330 °C and subsequent decay only at 450 °C whereas the latter decayed quickly at 310 °C and 435 °C [29]. From all these studies of physical characteristics, GNF_FePc is expected to act as better electrocatalysts in terms of morphology, stability, and good surface properties.

The morphological analyses of the synthesized composites via scanning electron microscopy are presented in Fig. 2. The commercial FePc exhibited irregular rectangular like solids in micrometer range (2 to 5 μm), as seen in Fig. 2 (a). After ball milling for 1 hour the size of Pc materials significantly decreased to nm range (~600 nm) as seen in 2 (b). Fig. 2 (c) showed GNF with rich fibrous structures. GNF_FePc (Fig. 2 (d)) showed a homogeneous mixture of FePc and graphite nanofibers with highly porous surfaces. Similarly in GNF_BM FePc, exhibited a homogenous mixture of porous nanofibers with BM FePc similar to that of 2 (d) except for the size difference observed for FePc after ball milling (2 (e)).

The energy dispersive X-ray spectra were measured to analyze the chemical composition of GNF_FePc composite. Fig. 3 shows the elemental analysis and mapping of the composite materials. EDX showed the presence of FePc and C with Fe, O and N for FePc. The weight percentages of carbon, iron and nitrogen in GNF_FePc composite measured by EDX were 79.4%, 13.8% and 5.13%, respectively, which are relatively closely related to estimated values calculated from molecular weight of FePc (C: 83.8%, Fe: 4.9%, and N: 9.8%). The mapping demonstrated the homogenous mixing of FePc and GNF. The weight percentages of the individual elements are given in the inset Table of Fig. 3.

The surface area of the synthesized catalysts was investigated by BET surface-area analysis and the nitrogen adsorption/desorption isotherms were shown in Fig. 4 with the corresponding surface properties in inset Table 2. FePc exhibit type IV isotherm with microporous nature which was already evidenced by FESEM. However, BM FePc showed hysteresis loop for high adsorption-desorption of N_2 with highly mesoporous nature. FePc had a surface area of about 1.084 $m^2 g^{-1}$, which increased to 4.775 $m^2 g^{-1}$ after ball milling. In contrast, GNF_FePc exhibit better isotherm than GNF_BM FePc which was highly unlikely. The BM FePc in nm scale must have covered the pores on GNF resulting in the better isotherm of GNF_FePc. Thus, GNF_FePc showed a high surface area of about 69.51 $m^2 g^{-1}$, which was reduced to 59.27 $m^2 g^{-1}$ in GNF_BM FePc. As mentioned earlier, this is mainly due to the agglomeration of ball milled phthalocyanines on the porous surface of graphite nanofibers and/or due to the over and re-deposition of BM FePc. Similar behaviors were observed for pore volume and pore size of GNF_ FePc and GNF_BM FePc [12].

3.2. Electrocatalytic performance

Catalytic activity (ORR and OER) of the synthesized composites were qualitatively estimated from the reduction/oxidation peak potentials measured in CV as given in Fig. 5. CV was analyzed in an organic medium (1 M LiTFSI in TEGDME) and the polarization curves were recorded in the range of 1.5 to 4.7 V vs. Li at a scan rate of 0.01 mV s^{-1}. During the first cycle, a sharp reduction peak at 2.7 and 2.6 V were clearly seen for GNF_FePc and GNF_BM FePc, respectively. This reduction peak corresponds to the reduction of oxygen which could be expressed as $Li^+ + O_2 \rightarrow 2e^- + Li_2O_2$ [37].

During oxidation, GNF_FePc and GNF_BM FePc produce a small peak at around 3.66 and 3.8 V, respectively, which corresponds to the OER reaction [40,41]. Another prominent peak is observed between 4.25 and 4.4 V from both GNF_FePc and GNF_BM FePc, indicating the decomposition of Li_2O_2 [42]. It has been reported that the existence of these two oxidation peaks are due to the decomposition of two electrochemically separate Li_2O_2 species such as bulk and interfacial Li_2O_2 [43]. It is conclusively verified that both the complexes are bifunctional and could catalyze both ORR and OER. Among the two synthesized compounds, GNF_FePc exhibit better catalytic performance with faster kinetics than GNF_BM FePc.

3.3. Li–O_2 battery application

The air cells were tested in a potential window of 2 to 4.3 V at 0.1 mA cm^{-2} and 1 atm O_2 atmosphere. The first cycle capacity GNF_FePc and GNF_BM FePc catalyzed air cells are shown in Fig. 6 (a) along with Ketjen black (KB) without any catalyst for standard comparison. GNF_FePc cell exhibited an open circuit potential of 3.2 V, which led to a maximum discharge capacity of ~5500 mAh g^{-1} with a first discharge plateau at 2.7 V. During charging the charge potential was 3 V with a maximum charging capacity of 5412 mAh g^{-1} at 3.3 V. The first cycle exhibited 99% reversibility with an overpotential of 0.6 V. Similarly, for GNF_BM FePc, the first

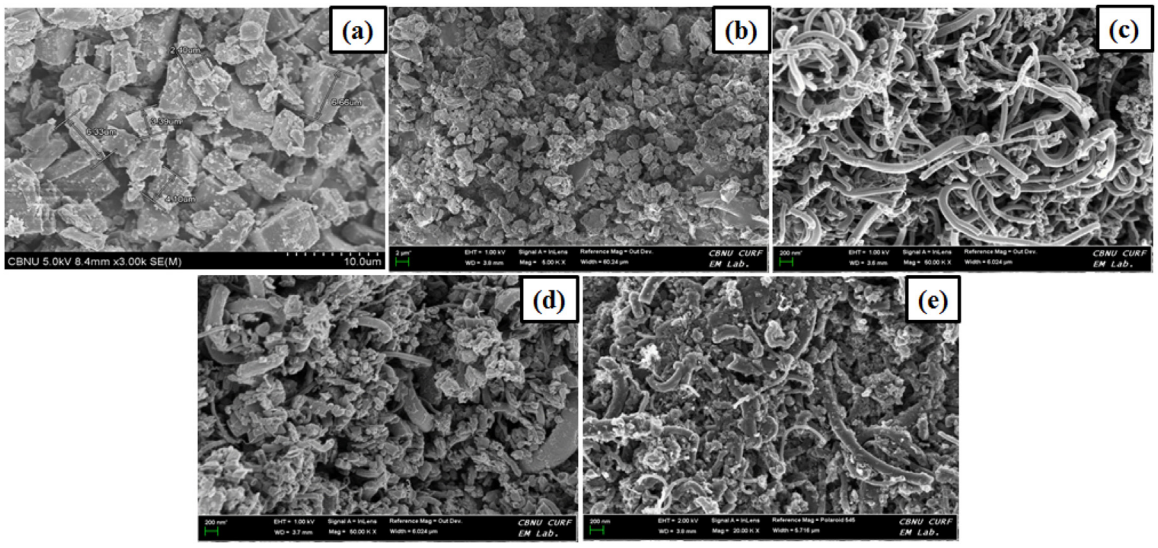

Fig. 2. Scanning electron microscopic images of (a) FePc, (b) Ball milled or BM FePc, (c) GNF, (d) GNF_FePc and (e) GNF_BM FePc composites.

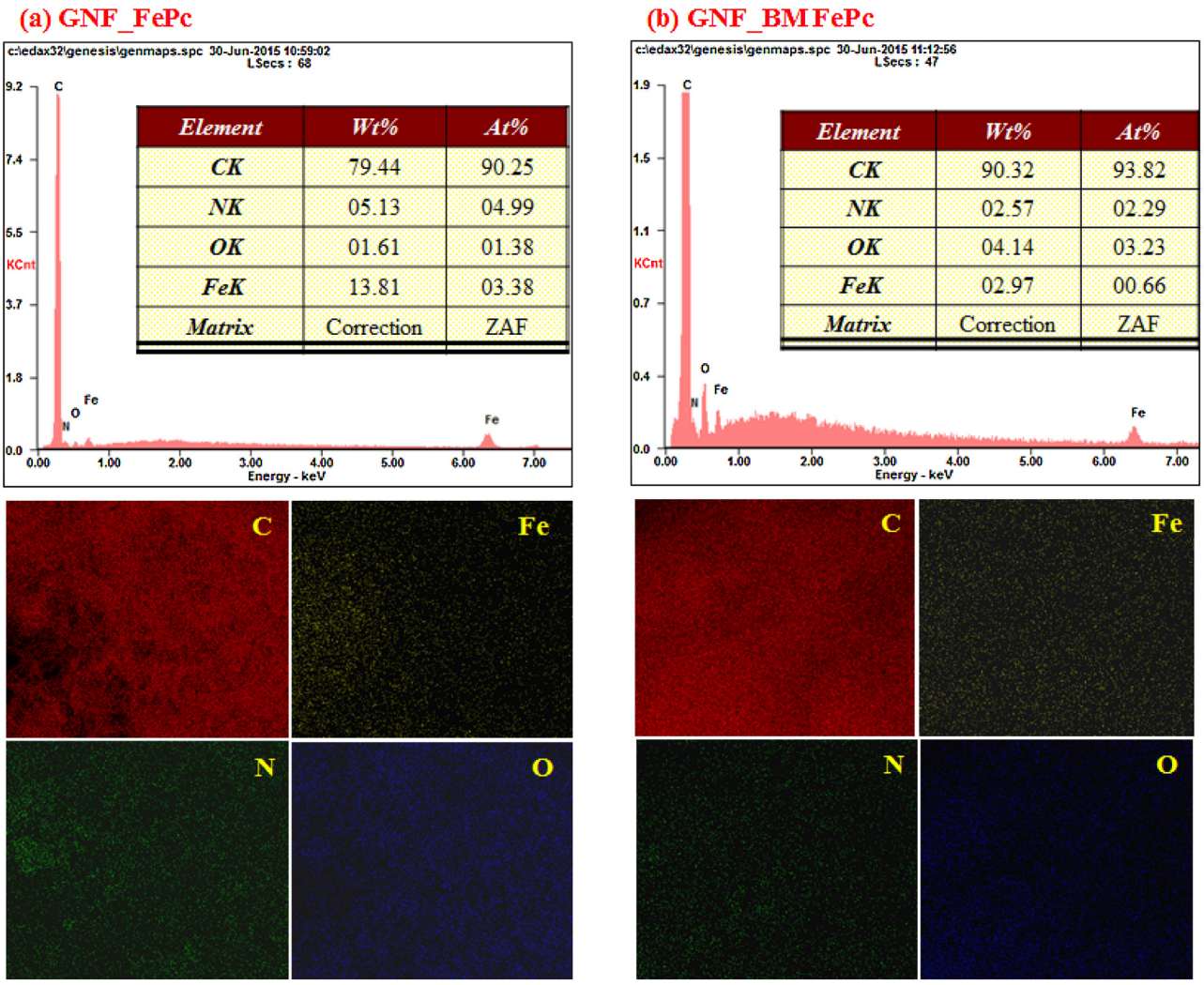

Fig. 3. Energy dispersed spectra and mapping of GNF_FePc and GNF_BM FePc; the corresponding elemental analyses are given in respective Table insets.

discharge begins to plateau at 2.7 V, leading to a maximum discharge capacity of 3453 mAh g^{-1} that resumed to 3214 mAh g^{-1} on charging with 93% reversibility. The overpotential was 0.8 V. GNF_FePc appeared to be the best among the two electrocatalysts with high capacity, capacity retention and reversibility with low overpotential. Nevertheless, both GNF_FePc and GNF_BM FePc electrocatalysts showed better discharge capacity, reversibility and overpotential when compared with the ketjen black (KB) carbon air cathode. Results reported here are better than published data [44] that employed cobalt Pc as electrocatalyst with $LiPF_6$ in acetonitrile electrolyte. Another recent report [45] with FePc supported on graphene nanosheets as a catalyst was also surpassed in performance by GNF_FePc in terms of battery performance mainly, cycle efficiency, discharge capacity and voltage gap.

Fig. 6 (b) shows the first four cycles of discharge-charge performance of a GNF_FePc catalyzed cell. This figure shows that even after 4 cycles with the full depth of discharge-charge, there is not much reduction in the capacity. The first cycle capacity and the fourth cycle capacity were found to be 5508 and 4800 $mAhg^{-1}$, respectively, with almost 100% reversibility for all the 4 cycles. It is obvious that the surface property of the FePc_GNF catalyzed air cathode remains good upon cycling, and they assist the proper formation and decomposition of the discharge product, Li_2O_2. The first four cycle capacity and the cell efficiency of GNF_FePc (and GNF_BM FePc for comparison) are provided in Fig. 6 (c and d) for a better understanding of the issue. Although the reversibility was very good, the capacity gradually decreased after every cycle. The main reason for the decrease in capacity after every cycle could be due to the slow clogging of pores upon cycling. The deep pores on the surface of the catalyst should have been clogged initially, so that gradually filled up after several cycles.

The main reason for the better reversibility in GNF_FePc compared to GNF_BM FePc could be explained by their surface properties. Electrocatalysts should provide more active sites for the promotion of Li_2O_2 formation and also highly porous in nature so that it is better for the diffusion of electrocatalysts and oxygen for the accomplishment of the formation reaction. In this case, it is obvious that GNF_FePc provides a higher surface area and large pore volumes compared to GNF_BM FePc, thus providing a better environment for the Li_2O_2 formation and decomposition reactions. The mesopores not only provided a way for oxygen and electrolyte diffusion but also helps to withhold a large amount of lithium peroxide during discharge.

Moreover, catalytic activity in metal phthalocyanines is said to be related to the relative energies of the d orbitals of the metal in

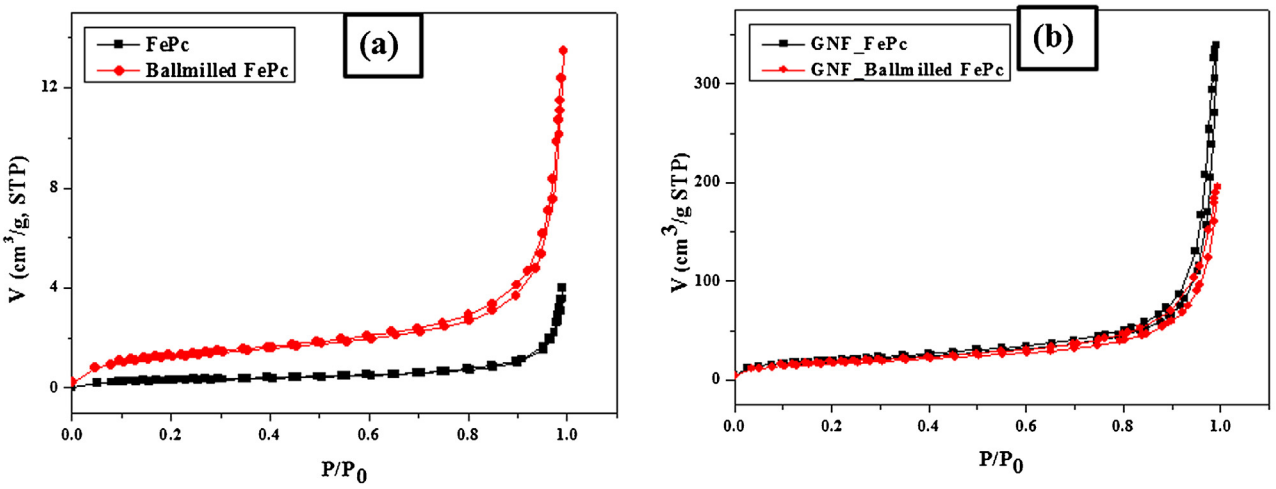

Table 2

Material	Surface area (m^2/g)	Pore Volume (cm^3/g)	Average Pore Size (nm)
FePc	1.084	0.0059	185.28
Ballmilled FePc (1hour)	4.775	0.0189	76.49
GNF_FePc	69.51	0.4946	163.19
GNF_Ballmilled FePc	59.27	0.2676	90.22

Fig. 4. N_2 adsorption/desorption isotherms of (a) FePc and BM FePc, and (b) GNF_FePc and GNF_BM FePc. The surface properties are derived and shown as an inset in Table 2.

the metal phthalocyanines, and their axial ligand [27]. According to the author [27], the presence of π donors as the fifth ligand on phthalocyanines increases their catalytic activity towards ORR resulting in low overpotential. Earlier studies [46,47] have also explained that Fe has half-filled d energy levels and exhibit maximum catalytic activity compared to other metals (Co, Ni, Mn, etc.) [29]. As a result, FePc catalyst has a high probability of electron transfer by providing a large number of active sites resulting in improved kinetics and low overpotential. Structural support is rendered by GNF and therefore the combined effect of both GNF and FePc in GNF_FePc catalyst exhibit improved catalytic activity inferred from Figs. 5 and 6.

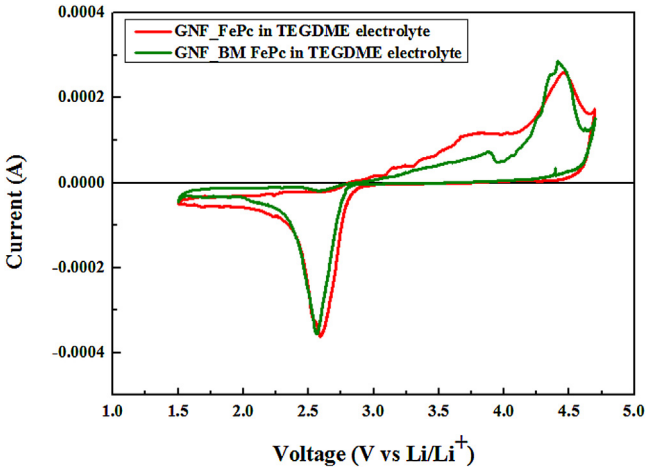

Fig. 5. Cyclic voltammogram of GNF_FePc and GNF_BM FePc catalysts measured in non–aqueous 1 M LiTFSI/TEGDME electrolytes using a Swagelok™ type cell.

For cyclability the Li–O_2 cells were tested by limiting the depth of discharge and charge since it is necessary for the practical application of air battery. Fig. 7 (a, b) shows the cycling of GNF_FePc and GNF_BM FePc at 500 mAh g^{-1} limited capacity. GNF_FePc and GNF_BM FePc exhibited steady cycling for 30 cycles each. But as expected, GNF_FePc was more stable than GNF_BM FePc with overpotential ranging between 0.6 to 1.4 V. The overpotential of GNF_BM FePc increased rapidly after 20 cycles which are not suitable for the battery application. For understanding, the cycle number vs. voltage for all the limited cycles is provided in Fig. 7 (c) along with cycle number vs. discharge capacity in 7(d). The better performance of GNF_FePc is attributed to its high surface area, and pore volume as explained earlier. In order to understand the surface changes that undergo upon cycling and to confirm the proper formation and decomposition of Li_2O_2, various studies were performed on the air cathodes.

3.4. Post characterization of O_2 cathodes

The post characterization studies include the post characterization X–ray diffraction and SEM analysis of the air cathodes. The tested cells were dismantled after discharge and charge processes in an argon-filled glovebox, and the electrodes were collected and

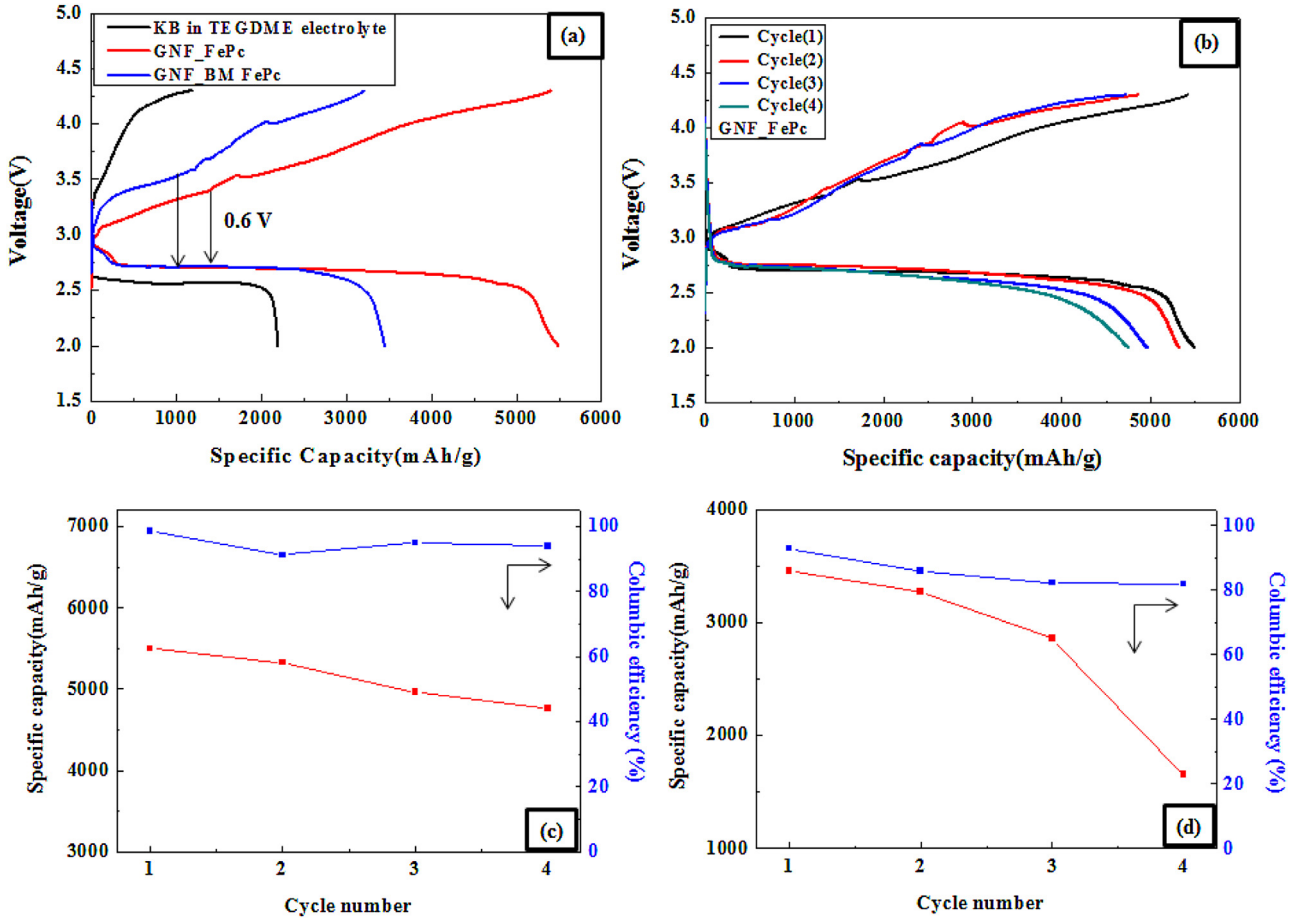

Fig. 6. (a) Charge/discharge curves of GNF_FePc and GNF_BM FePc at 0.1 mA cm^{-2}, (b) first four cycles of GNF_FePc catalyzed cell, (c) specific capacity and coulombic efficiency with respect to cycle number for GNF_FePc catalyst and (d) specific capacity and coulombic efficiency with respect to cycle number for GNF_BM FePc catalyst.

used for the post XRD and SEM characterization studies. The XRD patterns of pristine electrodes, the electrodes after first discharge and charge were evaluated in Fig. 8. Pristine electrode possessed the peaks of carbon and phthalocyanines with no additional peaks. After first discharge the electrode clearly shows new peaks that were formed as a result of the formation of Li_2O_2 and $LiOH.H_2O$ according to the standard JCPDS-25-0486 and 32-0564 (ORR reaction). There are no other secondary products observed other than Li_2O_2 that confirmed the proper formation of discharge products. After charging, all the Li_2O_2 peaks disappeared which demonstrated the proper decomposition of the discharge products upon recharge. The post characterization SEM also revealed proper formation and decomposition of Li_2O_2 on the electrode surface. Shown in Fig. 9 is the morphological analysis of the electrode used for battery testing during its first cycle. The pristine electrode of GNF_FePc in Fig. 9 (a) showed clear porous structure. After discharge, the pores are blocked, and a layer of Li_2O_2 deposition is seen all over the surface of the electrode. As the oxygen from outer atmosphere entered into the cathode and combined with lithium to form Li_2O_2, the solid products get deposited on the surface of the cathode as seen in Fig. 9 (b). After charging, the surface of electrode restored back to its original porous surface structure. That is, the solid products formed were decomposed, leaving the lithium back to its anode as oxygen was evolved. Thus both post-mortem analyses XRD and FESEM, evidenced the proper formation and decomposition of discharge products (Li_2O_2) with similar characteristics observed on electrode surfaces (pristine and after charging). Ironphthalocyanine had not been widely used for lithium air battery application even though it was proved to be an efficient ORR catalyst by various reports on fuel cells, supercapacitors, lithium ion batteries. This is the first report on graphite nanofibers–iron phthalocyanine combination as efficient electrocatalysts in lithium air battery applications to the best of our knowledge.

3.5. Electrochemical impedance spectroscopy

Wilcke et al. [5] had recently reported that the overpotential during discharge is caused by internal resistance and is dominated by the charge transport through the deposited Li_2O_2 at the end of discharge. In order to understand the internal resistance of the Li–O_2 battery, a series of electrochemical impedance spectra was measured at the initial stage of the assembled cells before testing, after first discharge and charge processes, as shown in Fig. 10. Fig. 10 (a) and (b) shows the Nyquist plot obtained for GNF_FePc and GNF_BM FePc catalyzed cells. From Fig. 10 (a) it could be interpreted that the resistance increases after first cycle discharge indicating the formation of lithium peroxide on the electrode surface. After charging the impedance returns to almost original confirming the decomposition of the earlier formed Li_2O_2.

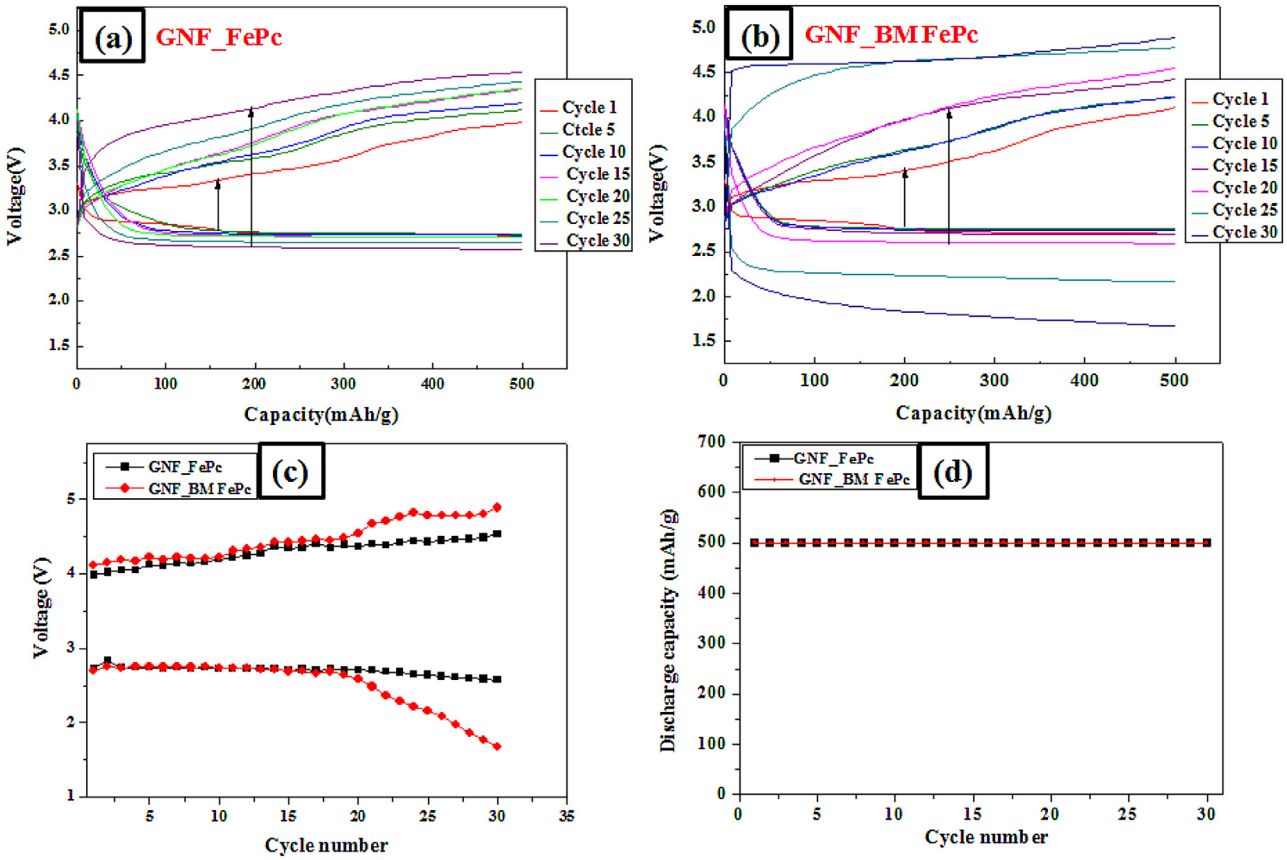

Fig. 7. Capacity limited cycling profiles of (a) GNF_FePc and (b) GNF_BM FePc; (c) Cycle number vs. voltage and (d) cycle number vs. discharge capacity of the synthesized composites.

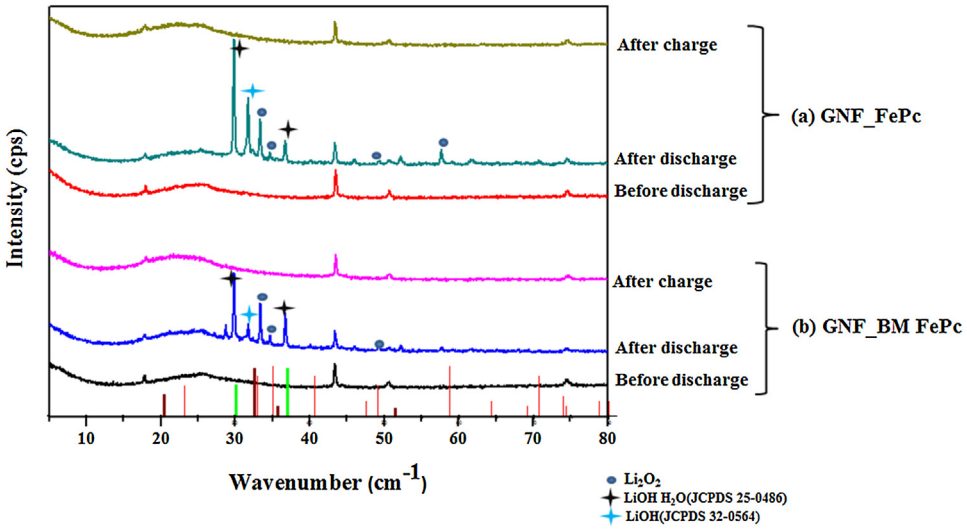

Fig. 8. XRD patterns of (a) GNF_FePc and (b) GNF_BM FePc catalyzed electrodes before and after first charge/discharge cycles.

Apparently, GNF_FePc catalyzed cell exhibit low resistance compared to GNF_BM FePc cell which is consistent with all other electrochemical characteristics.

4. Conclusions

GNF_FePc electrocatalysts was successfully developed as a suitable non–precious bifunctional air cathode catalyst by a simple and cost-effective method. The FePc compound materials (GNF_FePc and GNF_BM FePc) exhibited highly porous surfaces with large surface area and pore properties. In addition, the Raman and FTIR patterns revealed the π-π stacking of GNF and FePc. The structural stability in GNF_FePc aided the proper decomposition and recovery of reaction products upon cycling. The FePc catalyst was a mediator and increased the probability of electron transfer by providing a number of active sites which resulted in the

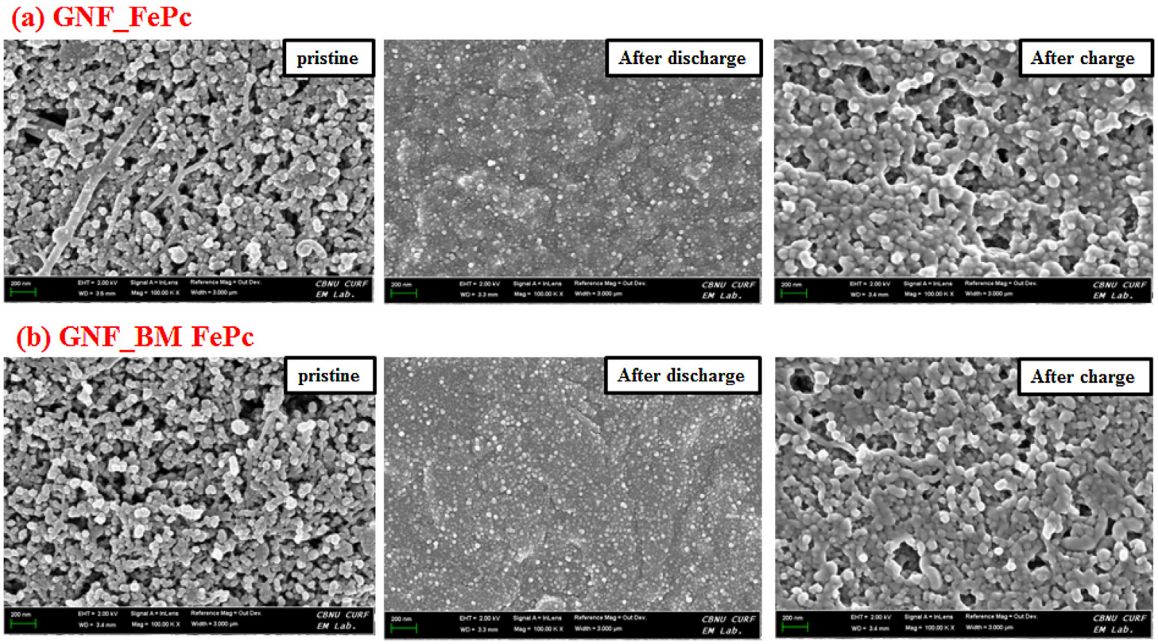

Fig. 9. SEM images of (a) GNF_FePc and (b) GNF_BM FePc catalyzed electrodes before and after first charge/discharge cycles.

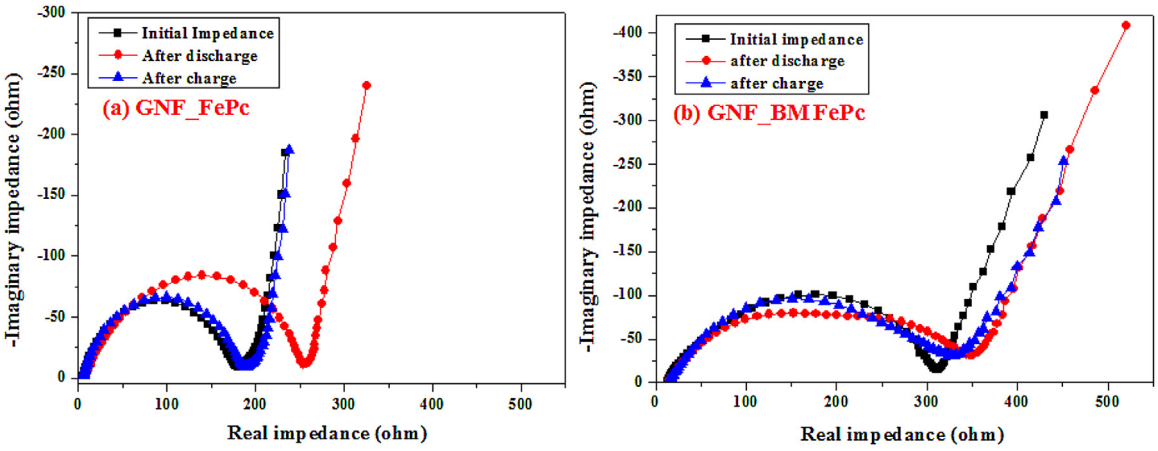

Fig. 10. Electrochemical impedance spectra of (a) GNF_FePc and (b) GNF_BM FePc catalyzed cells before and after first charge/discharge cycles.

reduction of oxygen (ORR) at low overpotential. The electrochemical performance showed better ORR and OER performance or bifunctional catalytic activity. When applied as air–cathode catalyst, GNF_FePc, exhibited superior performance in terms of capacity, cyclability and reversibility compared to GNF_BM FePc. Based on all the results, we conclude that FePc could be a potential non–noble electrocatalyst for future Li–O_2 batteries.

Acknowledgements

This work was supported by the Korea Institute of Energy Technology Evaluation and Planning (KETEP) and the Ministry of Trade, Industry & Energy (MOTIE) of the Republic of Korea (No. 20164030201070).

References

[1] K.M. Abraham, Z. Jiang, A Polymer Electrolyte-Based Rechargeable Lithium/Oxygen Battery, J. Electrochem. Soc. 143 (1996) 1–5.
[2] P.G. Bruce, S.A. Freunberger, L.J. Hardwick, J.M. Tarascon, Li-O_2 and Li-S batteries with high energy storage, Nat. Mat. 11 (2012) 19–29.
[3] T. Zhang, N. Imanishi, Y. Takeda, O. Yamamoto, Aqueous lithium/air rechargeable batteries, Chem. Lett. 40 (2011) 668–672.
[4] Y.C. Lu, B.M. Gallant, D.G. Kwabi, J.R. Harding, R.R. Mitchell, M.S. Whittingham, Y.S. Horn, Lithium-oxygen batteries: bridging mechanistic understanding and battery performance, Energy & Environ. Sci. 6 (2013) 750–768.
[5] G. Girishkumar, B. McCloskey, A.C. Luntz, S. Swanson, W. Wilcke, Lithium –air battery: promises and challenges, J. Phys. Chem. Lett. 1 (2010) 2193–2203.
[6] A. Zahoor, M. Christy, Y. Hwang, K.S. Nahm, Lithium-air battery: alternate energy resource for the future, J Electrochem. Sci. and Techn. 3 (1) (2012) 14–23.
[7] Y.C. Lu, H.A. Gasteiger, E. Crumlin, R. McGuire, Y.S. Horn, Electrocatalytic activity studies of select metal surfaces and implications in Li-air batteries, J. Electrochem. Soc. 157 (9) (2010) A1016–A1025.
[8] D.G. Kwabi, N. Ortiz-Vitoriano, S.A. Freunberger, Y. Chen, N. Imanishi, P.G. Bruce, Y.S. Horn, Materials challenges in rechargeable lithium-air batteries, MRS Bulletin 39 (5) (2014) 443–452.
[9] A. Kraytsberg, Y.J. Ein-Eli, Review on Li–air batteries—Opportunities, limitations, and perspective, J. Power Sources 196 (3) (2011) 886–893.
[10] X.M. Ren, S.S. Zhang, D.T. Tran, J. Read, Oxygen reduction reaction catalyst on lithium/air battery discharge performance, J. Mater. Chem. 21 (27) (2011) 10118–10125.

[11] A. Debart, J. Bao, G. Armstrong, P.G. Bruce, An O 2 cathode for rechargeable lithium batteries: the effect of a catalyst, J. Power Sources 174 (2) (2007) 1177–1182.
[12] A. Zahoor, M. Christy, Y. Hwang, Y.R. Lim, P. Kim, K.S. Nahm, Improved electrocatalytic activity of carbon materials by nitrogen doping, Applied catalysis B 147 (2014) 633–641.
[13] Y. Shao, S. Park, J. Xiao, J.G. Zhang, Y. Wang, J. Liu, Electrocatalysts for nonaqueous lithium-air batteries: status, challenges, and perspective, ACS Catal 2 (5) (2012) 844–857.
[14] R. Padbury, X. Zhang, Lithium–oxygen batteries—limiting factors that affect performance, J. Power Source 196 (2011) 4436–4444.
[15] A. Dobley, C. Morein, K.M. Abraham, Cathode Optimization for Lithium-Air Batteries, 208th ECS Meeting, Los Angeles, CA, USA, 2005 p Abstract#823.
[16] A. Zahoor, H.S. Jang, J.S. Jeong, M. Christy, Y. Hwang, K.S. Nahm, A comparative study of nanostructured α and (MnO 2 for lithium-oxygen battery application, RSC Adv. 4 (2014) 8973–8977.
[17] L. Trahey, C.S. Johnson, J.T. Vaughey, S.H. Kang, L.J. Hardwick, S.A. Freunberger, P.G. Bruce, M.M. Thackeray, Activated lithium-metal-oxides as catalytic electrodes for Li–O_2 cells, Electrochem. Solid State Lett. 14 (5) (2011) A64–A66.
[18] P. Sennu, M. Christy, V. Aravindan, Y.G. Lee, K.S. Nahm, Y.S. Lee, Two-Dimensional Mesoporous Cobalt Sulfide Nanosheets as a Superior Anode for a Li-Ion Battery and a Bifunctional Electrocatalyst for the Li–O_2 System, Chem. Mater. 27 (2015) 5726–5735.
[19] A. Zahoor, M. Christy, J.S. Jeon, Y.S. Lee, K.S. Nahm, Improved lithium oxygen battery performance by addition of palladium nanoparticles on manganese oxide nanorod catalysts, J.Solid State Electrochem. 19 (2015) 1501–1509.
[20] G. Gnana kumar, M. Christy, H. Jang, K.S. Nahm, Cobaltite oxide nanosheets anchored graphene nanocomposite as an efficient oxygen reduction reaction (ORR) catalyst for the application of lithium-air batteries, J. Power Sources 288 (2015) 451–460.
[21] Y. Shao, S. Park, J. Xiao, J. Zhang, Y. Wang, J. Liu, Electrocatalysts for Nonaqueous Lithium-Air Batteries: Status, Challenges, and Perspective, ACS Catal 2 (5) (2012) 844–857.
[22] R. Kou, Y. Shao, D. Wang, M.H. Engelhard, J.H. Kwak, J. Wang, V.V. Viswanathan, C. Wang, Y. Lin, Y. Wang, Enhanced activity and stability of Pt catalysts on functionalized graphene sheets for electrocatalytic oxygen reduction, Electrochem. Commun. 11 (2009) 954–957.
[23] E. Yoo, T. Okata, T. Akita, M. Kohyama, J. Nakamura, I. Honma, Enhanced Electrocatalytic Activity of Pt Subnanoclusters on Graphene Nanosheet Surface, Nano Lett. 9 (2009) 2255–2259.
[24] A. Zahoor, M. Christy, H. Jang, K.S. Nahm, Y.S. Lee, Increasing the reversibility of Li–O_2 batteries with caterpillar structured α–MnO_2/N–GNF bifunctional electrocatalysts, Electrochim. Acta 157 (2015) 299–306.
[25] C.C. Leznoff, A.B., Lever, A. B. P., Eds. VCH : Weinheim, Germany, 1989, 1993, 1996; Vols. 1-4.
[26] A.B. Sorokin, Phthalocyanine metal complexes in catalysis, Chem. Rev. 113 (2013) 8152–8191.
[27] O. Montellano, P. R., 3rd ed., KluwerAcademic/Plenum: New York, 2004.
[28] J. Zagal, Metallophthalocyanines as catalysts in electrochemical reactions, Coordination Chemistry Reviews 119 (1992) 89–136.
[29] J. Zagal, M. Pgez, Electrocatalytic activity of metal phthalocyanines for oxygen reduction, J. Electroanal. Chem. 339 (1992) 13–30.
[30] Y. Jiang, Y. Lu, X. Lv, D. Han, Q. Zhang, L. Niu, W. Chen, Enhanced catalytic performance of Pt-free iron phthalocyanine by graphene support for efficient oxygen reduction reaction, ACS Catal. 3 (2013) 1263–1271.
[31] L. Zhang, J.J. Zhang, D.P. Wilkinson, H.J. Wang, Progress in preparation of non-noble electrocatalysts for PEM fuel cell reactions, J. Power Sources 156 (2006) 171–182.
[32] W. Li, A. Yu, D.C. Higgins, B.G. Llanos, Z. Chen, Biologically inspired highly durable iron phthalocyanine catalysts for oxygen reduction reaction in polymer electrolyte membrane fuel cells, J. Am. Chem. Soc. 132 (2010) 17056–17058.
[33] A. Morozan, S. Campidelli, A. Filoramo, B. Jousselme, S. Palacin, Catalytic activity of cobalt and iron phthalocyanines or porphyrins supported on different carbon nanotubes towards oxygen reduction reaction, Carbon 49 (2011) 4839–4847.
[34] P.S. Harikumar, V.N. Sivasankara Pillai, Electrochemical studies on Metal phthalocyanines. Diss., Cochin University of Science and Technology, 1990.
[35] S. Zhang, H. Zhang, X. Hua, S. Chen, Tailoring molecular architectures of Fe-phthalocyanine on nanocarbon supports for high oxygen reduction performance, Journal of Materials Chemistry A 3 (2015) 10013–10019.
[36] Y. Chen, L. Chadderton, Improved growth of aligned carbon nanotube by mechanical activation, Journal of materials research 19 (2004) 2791–2794.
[37] Y. Chen, M. Bibole, R. Le Hazif, G. Martin, X-ray absorption studies of zirchonia polymorphs II effects of Y_2O_3 dopant on ZrO_2 structure, Physical Review B 48 (1993) 14.
[38] A. Kim, S. Lim, D.-H. Peck, S.-K. Kim, B. Lee, D. Jung, Preparation and Characteristics of SiO_x Coated Carbon Nanotubes with High Surface Area, Nanomaterials 2 (2012) 206–216.
[39] S. Baranton, C. Coutanceau, E. Garnier, J.M. Léger, How does α-FePc catalysts dispersed onto high specific surface carbon support work towards oxygen reduction reaction (orr)? J. Electroanal. Chem. 590 (1) (2006) 100–110.
[40] O.C. Laoire, S. Mukerjee, K.M. Abraham, Influence of nonaqueous solvents on the electrochemistry of oxygen in the rechargeable lithium- air battery, J. Phys. Chem. C 114 (2010) 9178–9186.
[41] O.C. Laoire, S. Mukerjee, K.M. Abraham, Elucidating the mechanism of oxygen reduction for lithium-air battery applications, J. Phys. Chem. C 113 (2009) 20127–20134.
[42] Jong Ju Lee, Mi Young Oh, Kee Suk Nahm, Effect of Ball Milling on Electrocatalytic Activity of Perovskite La0.6Sr0.4CoO3-(Applied for Lithium-Air Battery, Journal of The Electrochemical Society 163 (2) (2016) A244–A250.
[43] E.J. Nemanick, Electrochemistry of lithium–oxygen batteries using microelectrode voltammetry, J. Power Sources 247 (1) (2014) 26–31.
[44] C. Zhang, R. Hao, H. Yin, F. Liu, Y. Hou, Iron phthalocyanine and nitrogen–doped graphene composite as a novel non-precious catalyst for the oxygen reduction reaction, Nanoscale 4 (2012) 7326–7329.
[45] M.J. Trahan, Q. Jia, S. Mukerjee, E.J. Plichta, M.A. Hendrickson, K.M. Abraham, Cobalt phthalocyanine catalyzed lithium-air batteries, J. Electrochem. Soc. 160 (9) (2013) A1577–A1586.
[46] E. Yoo, H. Zhou, Fe-phthalocyanine supported by graphene nanosheet as catalyst in Li–air battery with the hybrid electrolyte, J. Power Sources 244 (2013) 429–434.
[47] J. Zagal, M. Paez, C. Fierro, Electrode Materials and Processes for Energy Conversion and Storage, in: S. Srinivasan, S. Wagner, H. Wrobloba (Eds.), Vol. 87–12, The Electro–chemical Society, Princeton, NJ, 1987, pp. p. 19.